THE UNIVERSITY of EDINBURGH

Edinburgh Research Explorer

A Reduced Gaussian Process Heat Emulator for Laser Powder Bed Fusion

Citation for published version:
Li, X & Polydorides, N 2021, A Reduced Gaussian Process Heat Emulator for Laser Powder Bed Fusion. in *Proceedings of the Changeable, Agile, Recongurable and Virtual Production Conference and the World Mass Customization & Personalization Conference: Towards Sustainable Customization: Bridging Smart Products and Manufacturing Systems.* Lecture Notes in Mechanical Engineering, SpringerLink, pp. 285-293, 8th Changeable, Agile, Reconfigurable and Virtual Production Conference, CARV 2021 and 10th World Mass Customization and Personalization Conference, MCPC 2021, Aalborg, Denmark, 1/11/21. https://doi.org/10.1007/978-3-030-90700-6_32

Digital Object Identifier (DOI):
10.1007/978-3-030-90700-6_32

Link:
Link to publication record in Edinburgh Research Explorer

Published In:
Proceedings of the Changeable, Agile, Recongurable and Virtual Production Conference and the World Mass Customization & Personalization Conference

General rights
Copyright for the publications made accessible via the Edinburgh Research Explorer is retained by the author(s) and / or other copyright owners and it is a condition of accessing these publications that users recognise and abide by the legal requirements associated with these rights.

Take down policy
The University of Edinburgh has made every reasonable effort to ensure that Edinburgh Research Explorer content complies with UK legislation. If you believe that the public display of this file breaches copyright please contact openaccess@ed.ac.uk providing details, and we will remove access to the work immediately and investigate your claim.

Download date: 08. Jun. 2022

A Reduced Gaussian Process Heat Emulator for Laser Powder Bed Fusion

Xiaohan Li(✉) and Nick Polydorides

School of Engineering, University of Edinburgh, Edinburgh, UK
xiaohan.li@ed.ac.uk

Abstract. Laser Powder Bed Fusion (LPBF) is a promising additive manufacturing technique used for realizing complex and bespoke designed metal parts. Despite its good performance, its quality assurance is still hampered by the absence of in-process optimization and control. In this sense, real-time thermal analysis can facilitate fault predictions and rectifications. High-fidelity three-dimensional thermal modelling with the Finite Element Method (FEM) is generally time-consuming since the heat transfer equation is nonlinear and high-dimensional. The challenge is thus to compute fast, reliable and accurate thermal predictions that capture the nonlinearity triggered by the phase changes of the part during printing. Gaussian Process (GP) with Isomap dimension reduction is investigated to find and predict the low-dimensional representations of the high-dimensional thermal profiles in FEM without intricate processing. Based on these representations, the high-dimensional predictions are then approximated using localized radial basis functions. To validate the performance of this reduced GP heat emulator, a heat simulation during fabricating an Aluminum object is performed to compare FEM-based temperature calculations against reduced GP emulations. Retaining 0.06% of the original model dimension the execution time per temperature profile is 0.70s on average achieving a 95.07% reduction, while maintaining at least 85% accuracy (with respect to the FEM simulation) for 96.80% of the thermal profile queries and at least 80% for 89.38% of the thermal history queries. With this encouraging performance, the reduced GP heat emulator can be a step forward in online defect prediction, process optimization and closed-loop control in LPBF.

Keywords: Finite element method · Gaussian process · Laser powder bed fusion · Nonlinear dimension reduction · Transient thermal model

1 Introduction

Additive manufacturing (AM) has driven a revolution of the manufacturing industries. Though it has promising future, the quality of printed parts is not assured and online process dynamic analysis is imperative. Real-time thermal history simulation is an essential part of process dynamics analysis for a thermal-driven AM like LPBF, since it describes the transient temperature gradient in

© Springer Nature Switzerland AG 2022
A.-L. Andersen et al. (Eds.): CARV 2021/MCPC 2021, LNME, pp. 285–293, 2022.
https://doi.org/10.1007/978-3-030-90700-6_32

localised melting and cooling [1] and is used in the predictions of residual stress, microstructure, defect and mechanical property [2,3].

There are an extensive amount of literatures on thermal models of AM validated by experiments. A nonlinear temperature simulation of Selective Laser Melting (SLM) utilizing FEM was validated in [1] by an experiment with AlSi10Mg powder and in [4] by the AM benchmark experimental set AMB2018-02 with anisotropic thermal conductivity. Though FEM produces high-fidelity thermal profiles, the nonlinearity, fine spatial and temporal resolution entail a high time cost constraining in-situ operations. To reduce the degrees of freedom, adaptive meshing [5] and decomposed domain [6] were applied, both of which only slightly reduce the time cost. Alternatively, a statistical Surrogate Model (SM) is considered as a reasonable trade-off between accuracy and time cost. Trained by data generated from a high-fidelity physics-based model, it makes fast predictions for given design points [7]. Lening et al. designed a Gaussian-process-constrained general path model in [8] describing heterogeneous discrepancies between low-fidelity and high-fidelity thermal modelling in AM. Mriganka et al. [9] predicted thermal histories almost in real-time using deep learning with different part sizes and same printing parameters based on a unique design of heat influence zone.

In this paper, the reduced-dimensional GP with Isomap scheme is developed to emulate the thermal modelling of LPBF with Al materials. With a given pair of laser power and scan speed, the high-dimensional thermal profiles are constructed by their low-dimensional representations predicted by GP emulators. One prediction takes around 0.7026 s reduced from 14.2617 s on average regardless of the degrees of freedom. 95.07% of execution time is saved while maintaining acceptable accuracy (around 96.8% of predictions having relative error less than 15%). This SM provides real-time thermal histories needed for in-situ optimizations and controls.

2 Thermal Simulator and Emulator

2.1 Numerical Solver with FEM

The temperature $u := u(x,t)$ within a computational domain $\Omega \subset \mathbb{R}^3$ is governed by the time-dependent, nonlinear heat transfer equation

$$\rho c \frac{\partial u}{\partial t} + \rho L \frac{\partial f_p}{\partial t} - \nabla \cdot \bar{\kappa} \nabla u = 0, \quad \text{in } \Omega \times [0, t_f], \tag{1}$$

where ρ, c and $\bar{\kappa}$ are respectively the temperature dependent density, heat capacity and conductivity of the materials, L is the latent heat of the materials, while $x := (x_1, x_2, x_3)$ and t are the spatial and temporal coordinates. The thermal conductivity is modelled as a symmetric, positive definite tensor field, and thus the elliptic term in (1) has the form $\nabla \cdot \bar{\kappa}(x) \nabla u := \sum_{i,j=1}^{3} \frac{\partial}{\partial x_i} \left[\kappa_{ij}(x) \right] \frac{\partial u}{\partial x_j}$. The material-dependent phase change function is $f_p(u) = \frac{1}{1+\exp\left(-\beta(u-u_m)\right)}$ with the

melting temperature u_m and $\beta > 0$ controlling the smoothness. The boundary of Ω is split into three disjoint regions as $\Gamma = \Gamma_t \cup \Gamma_s \cup \Gamma_b$ spanning the top, side and bottom surfaces respectively, while $\hat{\mathbf{n}}$ denotes the outward unit normal on Γ. We apply a time-varying sintering heat source $q(x;t)$ moving on a fixed trajectory embedded on Γ_t. In effect, the imparted heat flux is expressed by the Neumann boundary condition [1]

$$\bar{\kappa}\nabla u \cdot \hat{\mathbf{n}} = q(x;t) \quad \text{where} \quad q(x;t) \doteq \frac{2aP}{\pi r_q^2} \exp\left(-\frac{2\sum_{i=1}^{3}\left(x_i - x_i^q(t)\right)^2}{r_q^2}\right) \quad x \text{ on } \Gamma_t, \tag{2}$$

where a is the laser energy absorptivity, P is laser power, $x^q(t)$ is the position of beam center, and r_q is the effective laser beam radius. The bottom surface of the powder bed is on a temperature controlled platform hence a Dirichlet condition

$$u(x,\cdot) = u_b, \quad x \text{ on } \Gamma_b, \tag{3}$$

where u_b is the temperature of the building platform. On the top and side surfaces, the heat loss due to convection q_c and radiation q_r leads to

$$-\bar{\kappa}\nabla u \cdot \hat{\mathbf{n}} = q_c + q_r, \quad q_c(x,t) = h(u - u_a), \quad q_r(x,t) = \sigma_s \varepsilon (u^4 - u_a^4), \quad x \text{ on } \Gamma_s \cup \Gamma_t, \tag{4}$$

where $h > 0$ is the coefficient of heat convection, σ_s is the Stefan-Boltzmann constant, ε is the emissivity and u_a is the ambient temperature [11,12]. The dynamical equations (1)–(4) together with the initial condition $u(\cdot,0) = u_0$ and the parameter values in Table 1 admit a unique solution $u(x,t) \in \Omega \times [0,t_f]$.

Table 1. Model parameters used in the FEM simulation as in [1].

Symbol	Definition	Value	Unit
a	Absorptivity	0.09	–
ε	Emissivity	0.04	–
r_q	Laser spot radius	35	μm
u_a	Ambient temperature	20	$^\circ C$
u_b	Building platform temperature	200	$^\circ C$
h	Heat convection coefficient	10	W/(m^{2}K)
σ_s	Stefan-Boltzmann constant	5.67×10^{-8}	W/(m^{2}K^4)
-	Powder layer dimension	$1.54 \times 0.7 \times 0.1$	mm

Following a Galerkin approach the continuous temperature field is projected on a finite dimensional space of piecewise linear functions in space and time [4]. On a discretised domain with d nodes, we arrive at the nonlinear system for the FEM coefficients $u_t \in \mathbb{R}^d$ of the temperature at time steps t as

$$A(u_t)u_{t+1} = b(u_t), \quad \text{for} \quad t = 0, 1, \ldots, t_f, \tag{5}$$

where $A \in \mathbb{R}^{d\times d}$ and $b \in \mathbb{R}^d$ both depend non-linearly on the temperature. The nonlinear matrix equation for u_{t+1} can be solved iteratively via Picard iterations until the residual $\|r(u)\| = \|A(u)u - b(u)\|$ below a very small constant [13].

2.2 Reduced Gaussian Processes

Gaussian Process Emulators (GPEs) with isomap dimension reduction are proposed to make almost instantaneously temperature predictions irrespectively of the dimension of FEM. Before outlining our method we fix our notation. For a matrix X, X_i denotes the i-th column, X_i^T the corresponding row and X_{ij} the (i,j)-th element. For a vector y, y_i denotes the i-th element.

In our case the triplet of beam speed v, power P, and time t are input parameters controlling the printing process. We thus consider an input matrix X whose i-th column is $(v_i, P_i, t_i)^T$. Repeating the FEM simulation in (5) for $n \gg 3$ sampling points yields matrix $X \in \mathbb{R}^{3\times n}$ and a respective FEM snapshots matrix $F \in \mathbb{R}^{d\times n}$ whose i-th column is $u(X_i)$. We then center the elements of the rows of F to a zero mean output matrix $Y \in \mathbb{R}^{d\times n}$ by $Y_i^T = F_i^T - \frac{1}{n}F_i^T\mathbf{1}$. We assume that the elements in the vector $Y_i^T \in \mathbb{R}^n$ satisfy a discrete Gaussian process with zero mean and positive definite covariance matrix $\Sigma = C + \sigma^2 I \in \mathbb{R}^{n\times n}$ as

$$Y_i^T \approx \mathcal{GP}(X), \quad \hat{C}_{ij} \approx k(X_i, X_j; \theta) \doteq \theta_0 \exp(-\|X_i - X_j\|^2/2\theta_1). \tag{6}$$

where $k(x, x'; \theta)$ is the squared exponential function (kernel) and hyper-parameters $\theta = [\theta_0, \theta_1, \sigma^2]^T$ are strictly positive obtained via maximum likelihood estimation, we can then predict $\hat{y}_i$ for a test input $\tilde{x} \in \mathbb{R}^3$ with variance $\mathrm{Var}(\hat{y}_i)$

$$\hat{y}_i = k_x^T \Sigma^{-1}(Y_i^T)^T, \quad \mathrm{Var}(\hat{y}_i) = \theta_0 - k_x^T \Sigma^{-1} k_x, \quad \text{for} \quad i = 1, \ldots, d, \tag{7}$$

where $k_x := \left[k(X_1, \tilde{x}; \hat{\theta}), \ldots, k(X_n, \tilde{x}; \hat{\theta})\right]^T$ [14].

It is easy to see that applied to a high-dimensional discrete model, evaluating (7) d times becomes cumbersome. To alleviate this computational burden, we seek to construct a low-dimensional representation $Z \in \mathbb{R}^{r\times n}$ with $r \ll d$ of the data matrix $Y \in \mathbb{R}^{d\times n}$ with Isomap approach so that in predicting $u(\tilde{x})$ requires r instead of d GPE evaluations. Isomap dimension reduction captures the nonlinear dependence of the data in Y on the parameters in X based on the symmetric dissimilarity matrix $D \in \mathbb{R}^{n\times n}$. D_{ij} is the shortest path distance between Y_i and Y_j points computed via the Floyd–Warshall algorithm [15] in a graph where edges are built between neighbour points with weights equal to Euclidean distance. The points are assumed to belong in the same neighbourhood if $\|Y_i - Y_j\|$ is less than or equal to a chosen constant. Forming the $n \times n$ matrix

$$Q = -\frac{1}{2}H(D \circ D)H, \quad \text{where} \quad H = I - \frac{1}{n}\mathbf{1}\mathbf{1}^T \tag{8}$$

and $\circ$ denotes the Hadamard product. From the eigendecomposition $Q = E\Lambda E^T$ we can compute a r-rank approximation basis with columns $Z_i = \Lambda_{ii}^{\frac{1}{2}} E_i$ for $i = 1, \ldots, r$. Effectively, for a test input $\tilde{x}$, we solve

$$\hat{z}_i = k_x^T \Sigma^{-1} (Z_i^T)^T, \quad \text{for} \quad i = 1, \ldots, r, \tag{9}$$

where k_x and Σ are trained by the reduced data $\{(X_i, Z_i)\}_{i=1}^n$. To extrapolate for the high-dimensional temperature solution we compute the weights $w = [w_1, \ldots, w_n]^T$ via localized radial basis functions

$$w_i \propto \exp\Big(-\frac{\|\hat{z} - Z_i\|^2}{\xi^2}\Big), \quad \text{such that} \quad \sum_{i=1}^{n} w_i = 1, \tag{10}$$

for a constant parameter $\xi > 0$, and thereafter the prediction $\hat{y}(\tilde{x}) = Yw$.

3 Results

To demonstrate the performance of our method we consider a small scale numerical study on the thermal modelling involving a cuboid Aluminium structure consisted of four adaptive layers. Three straight laser trajectories are simulated on the top surface as shown in Fig. 1. The computational times for each layer are provided in Table 2 running Matlab R2020b on an Intel Core i7 CPU at 2.6 GHz, 16 GB RAM computer.

The high-fidelity FEM-based heat simulation with fine spatio-temporal discretisation has been utilised to generate training data for the reduced-dimensional GP emulation. The accuracy of this surrogate model depends on finding representative training data so as to guarantee an accurate response surface. In the absence of the information on the printing parameter distribution, we applied a uniform grid search in the admissible range of laser power: 200–400 W, scan speed: 200–400 mm/s and time: 0–6 ms to obtain 1844 pairs of uniformly sampled $X_j^{(i)} = [P_j^{(i)}, v_j^{(i)}, t_j^{(i)}]^T$ and the corresponding FEM temperature snapshots $Y_j^{(i)}$ forming the training dataset $\{X_j^{(i)}, Y_j^{(i)}\}_{j=1}^{1844}$ in i-layer domain for $i = 1, \cdots, 4$.

Fig. 1. The laser scanning pattern on the i-th layer surface, indicating the location of the reference points s_{i1}, s_{i2}, and s_{i3}.

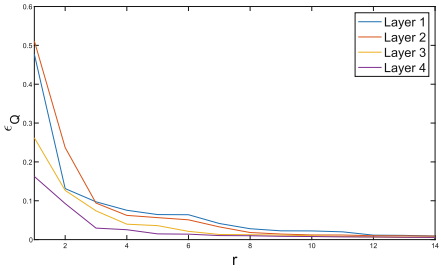

Fig. 2. The relative reduction error ϵ_Q for different reduced dimensions r.

In order to trace the lower-dimensional representation by Isomap method, we require the neighbourhood size and the reduced dimension r. While the neighbourhood size is chosen to ensure the connectivity of the constructed graph, the reduced dimension r is heuristically chosen to keep low relative reduction error $\epsilon_Q = \frac{\|Q - Z^T Z\|}{\|Q\|}$. The decreased trends of ϵ_Q with r for all four domains are shown in Fig. 2 making $r = 8$ a reasonable choice for our setup.

A set of predictions are computed for 219 testing inputs, aimed to assess the prediction speed and accuracy. Collectively, these results suggest that about 96.80%, 87.44%, 61.87% and 19.18% of predictions have respective relative errors that are no bigger than 15%, 10%, 5% and 1%. A representative subset of these result at $P = 255\,\mathrm{W}$ and $v = 215\,\mathrm{mm/s}$ are illustrated in Fig. 3. It compares FEM

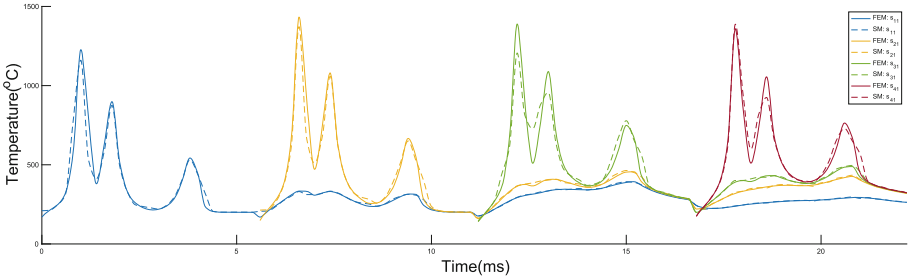

(a) Thermal history at s_{11}, s_{21}, s_{31} and s_{41}

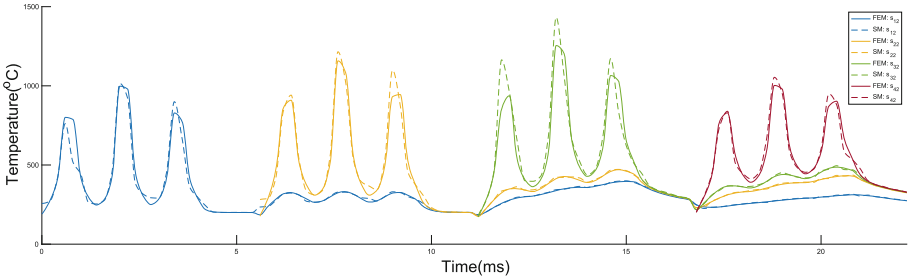

(b) Thermal history at s_{12}, s_{22}, s_{32} and s_{42}

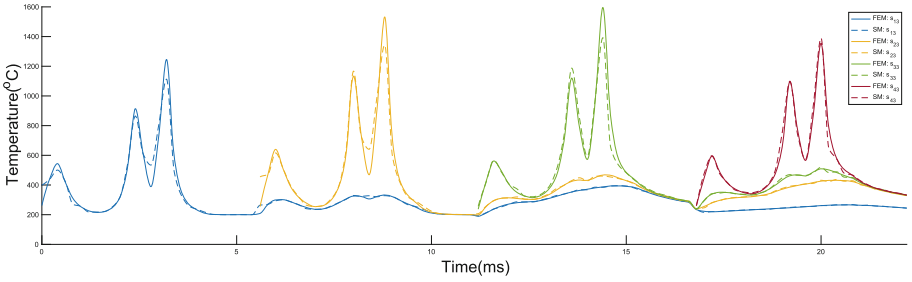

(c) Thermal history at s_{13}, s_{23}, s_{33} and s_{43}

Fig. 3. The thermal histories from FEM and SM with $P = 255\,\mathrm{W}$ and $v = 215\,\mathrm{mm/s}$

simulation and SM prediction at the 12 reference points $\{s_{i1}, s_{i2}, s_{i3}\}$ for $i = 1, \cdots, 4$ as in Fig. 1 throughout the entire printing, where each layer takes about 6 ms to print.

Besides these 12 reference positions, thermal history predictions at 744 other locations were tested indicating that 47.45%, 77.82% and 89.38% of those have relative errors bounded below 10%, 15% and 20% respectively. The computational times in our SM are listed in Table 2. Note that only the prediction is required online. The prediction time alone costs, on average, 95% less than the more accurate FEM simulation.

Table 2. The time cost of SM and the reduction of execution time.

Number of Layers	Degrees of Freedom	Data Generation(hr)	Training(min)	Average Execution Time	
				FEM(s)	Prediction(s)
1	14219	3.0857	34.5171	6.0242	0.7206
2	25201	7.2799	30.7677	14.2124	0.6868
3	26633	9.3825	28.7027	18.3472	0.7093
4	26841	9.3135	38.1348	18.4629	0.6936

The proposed approach couples data-driven machine learning and nonlinear model order reduction to expedite thermal simulation in LPBF. In principle, the proposed reduced GPEs and the FEM simulator are also applicable to other types of thermal-driven AM, since we can modify the heat source and its trajectory or indeed consider materials with different thermal properties that also undergo phase transitions without changing the main structure of our computational models and algorithms. Our numerical tests showed that 96.8% of temperature profile predictions at a given time have relative error less than 15% and 89.38% of thermal history predictions at the control points have relative errors less than 20%. Predictions at arbitrary times after the start of the printing process are computed fast at around 0.7 s. Further, as the domain is augmented layer by layer the complexity of our computations is controlled since the Isomap scheme compresses the amount of Gaussian processes required to a fairly small number ($r = 8$). Also, the process of pre-processing is fixed for different object geometries. With different scanning patterns, a related representative training dataset is required but no additional trajectory-based design is needed. Less cumbersome design and computation means more swift applications in thermal analysis, planning and decision making.

4 Conclusions

A time-efficient SM based on the reduced GP with Isomap method is developed to predict the thermal history of LPBF from laser power and scan speed, the

pre-processing process of which is less geometry-dependent in dealing the redundancy and cyclic heating and cooling. The showcase of fabricating a cuboid with Al material is made to assess the performance. The SM shows encouraging performance in predicting temperature profiles by reducing 95.07% of time cost (from 14.3 s to 0.7 s) with high prediction accuracy (>85% for 96.80% of testings). Thermal history predictions for 89.38% of tested positions have relative error less than 20%. Since a 3D printer can alter laser power and scan speed during the printing process, the SM takes one step further in quality assurance by possible in-situ optimizations and controls. While this GP surrogate model allows us to bypass FEM's long time-marching process to compute the temperature, the accuracy of SM highly depends on finding a representative training dataset, and only test inputs within the window of interest can be predicted.

References

1. Li, Y., Gu, D.: Parametric analysis of thermal behavior during selective laser melting additive manufacturing of aluminum alloy powder. Mater. Des. **63**, 856–867 (2014)
2. Tong, Z., et al.: Laser additive manufacturing of FeCrCoMnNi high-entropy alloy: Effect of heat treatment on microstructure, residual stress and mechanical property. J. Alloy. Compd. **785**, 1144–1159 (2019)
3. Moran, T., Warner, D., Phan, N.: Scan-by-scan part-scale thermal modelling for defect prediction in metal additive manufacturing. Add. Manuf. **37**, 101667 (2020)
4. Kollmannsberger, S., Carraturo, M., Reali, A., Auricchio, F.: Accurate prediction of melt pool shapes in laser powder bed fusion by the non-linear temperature equation including phase changes. Integrating Mater. Manuf. Innovation **8**(2), 167–177 (2019). https://doi.org/10.1007/s40192-019-00132-9
5. Patil, N., Pal, D., Stucker, B., et al.: A new finite element solver using numerical eigen modes for fast simulation of additive manufacturing processes. In: Proceedings of the Solid Freeform Fabrication Symposium, pp. 12–14 (2013)
6. Moran, T., et al.: Utility of superposition-based finite element approach for part-scale thermal simulation in additive manufacturing. Add. Manuf. **21**, 215–219 (2018)
7. N. V. Queipo et al. "Surrogate-based analysis and optimization". In: Progress in aerospace sciences 41.1 (2005), pp. 1–28
8. Wang, L., et al.: Meta-modeling of high-fidelity FEA simulation for efficient product and process design in additive manufacturing. Add. Manuf. **35**, 101211 (2020)
9. Roy, M., Wodo, O.: Data-driven modeling of thermal history in additive manufacturing. Add. Manuf. **32**, 101017 (2020)
10. Tenenbaum, J.B., De Silva, V., Langford, J.C.: A global geometric framework for nonlinear dimensionality reduction. Science **290**(5500), 2319–2323 (2000)
11. Sheikhi, M., Ghaini, F.M., Assadi, H.: Prediction of solidification cracking in pulsed laser welding of 2024 aluminum alloy. Acta Mater. **82**, 491–502 (2015)
12. Ramanathan, K., Yen, S.: High-temperature emissivities of copper, aluminum, and silver. JOSA **67**(1), 32–38 (1977)
13. Larson, M.G., Bengzon, F.: The finite element method: theory, implementation, and practice. Texts Comput. Sci. Eng. **10**, 23–24 (2010)

14. Xing, W., Shah, A.A., Nair, P.B.: Reduced dimensional Gaussian process emulators of parametrized partial differential equations based on Isomap. In: Proceedings of the Royal Society A: Mathematical, Physicaland Engineering Sciences, vol. 471 no. 2174, p. 20140697 (2015)
15. Wu, Y., Chan, K.L.: An extended Isomap algorithm for learning multi-class manifold. In: Proceedings of 2004 International Conference on Machine Learning and Cybernetics (IEEE Cat. No. 04EX826), vol. 6, pp. 3429–3433. IEEE (2004)